ACS OMEGA

http://pubs.acs.org/journal/acsodf

Article

Preparation and Performance of Microencapsulated Sealing Material for Coal Mine Gas Drainage

Qin RongRong, Zhang Chao,* Jiang Bingyou, Liu Ting, Chang Jie, and Fan Fuhuai

Cite This: *ACS Omega* 2022, 7, 47821−47831

Read Online

ACCESS | Metrics & More | Article Recommendations

ABSTRACT: The performance of coal mine gas extraction borehole sealing material plays an essential role in the efficiency of gas extraction. Microcapsule technology was proposed to delay the expansion time of sealing materials to address the ineffective expansion of cement-based sealing materials in hydration. Based on conventional cement-based sealing materials, delayed-expansion microcapsules were prepared by phase separation with ethyl cellulose (EC) as the capsule wall material and montmorillonite (MMT) as the core material. A single-factor experiment showed that the delayed-expansion microcapsule had the best comprehensive effect when the EC content was 3%, the stirring rate was 400 rpm, the MMT content was 3.5%, and the core−wall ratio (CWR) was 10:3. Second, the slow release effect of the cement samples under the action of microcapsules is remarkable through physical tests. In addition, the triaxial compression test results show better mechanical properties of the delayed-expansion sealing materials. Then, nuclear magnetic resonance scanning was applied to the coal samples injected with different sealing materials. It was found that the proportions of macropores and mesopores in the total pore volume in the coal sample at 50 and 100 mm from the borehole wall decreased by 12.28 and 11.82%, respectively, indicating that the delayed-expansion sealing material has a better sealing effect.

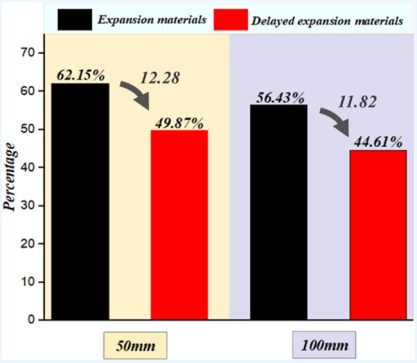

1. INTRODUCTION

Coal supports more than 50% of industrial development in China, but more than 90% of domestic coal mining occurs underground, and 22% occurs in coal and gas outburst-prone mines.[1−3] With the increase of the coal mining depth, the coal seam gas pressure and contents gradually increase as geological conditions change.[4−7] Gas disasters have become the leading cause of coal mining accidents and have inflicted the worst damage. These conditions are the main reason why China has become the country at the highest risk of coal and gas outburst disasters.[8,9]

The most effective way to prevent and control coal or gas outbursts and decrease the probability of their occurrence is gas extraction.[10−12] Gas extraction using boreholes is the most effective and widely used gas extraction technique, and it can reduce the coal gas pressure and content to reduce the gas outburst danger.[13−15] However, its overall efficacy in gas extraction is unsatisfactory.[16] In China, the concentration of the drainage holes will attenuate to below 30% after a short gas drainage period in most coal mines.[17−19] In borehole pressure tests, the rate of effective gas emission of less than 50% will result in an inefficient gas extraction process.[20] The effective way to improve gas extraction efficiency is by improving the performance of sealing materials used in boreholes.[21−23]

Borehole sealing materials mainly include clay sealing materials, ordinary cement materials, polyurethane materials, new sealing materials, and modified cement materials.[24,25] Initially, clay materials were used for sealing gas extraction boreholes due to the difficulty of construction, shallow sealing depth, and easy softening of materials, so clay has been replaced by cementitious materials.[22,26,27] Cementitious materials allow control over the grouting depth. However, they shrink and fracture during solidification, thus reducing the effectiveness of borehole sealing.[28−30] Polyurethane sealing materials have been used for their simple operation process, fast speed, and large expansion ratio. However, gas drainage boreholes sealed with polyurethane have poor compressive performance in humid environments in practical applications.[31,32]

Hu et al.[33] investigated the mechanism of powder-based blocking of fractures and used powder to seal the fractures around a gas extraction borehole. Hao et al.[34] studied the physical properties of silica sol and the sealing performance of the fractures around gas drainage boreholes in a coal body. Wang et al.[35] proposed a dynamic leak prevention method for gas extraction boreholes with short sealing depths and

Received: August 31, 2022
Accepted: November 23, 2022
Published: December 14, 2022

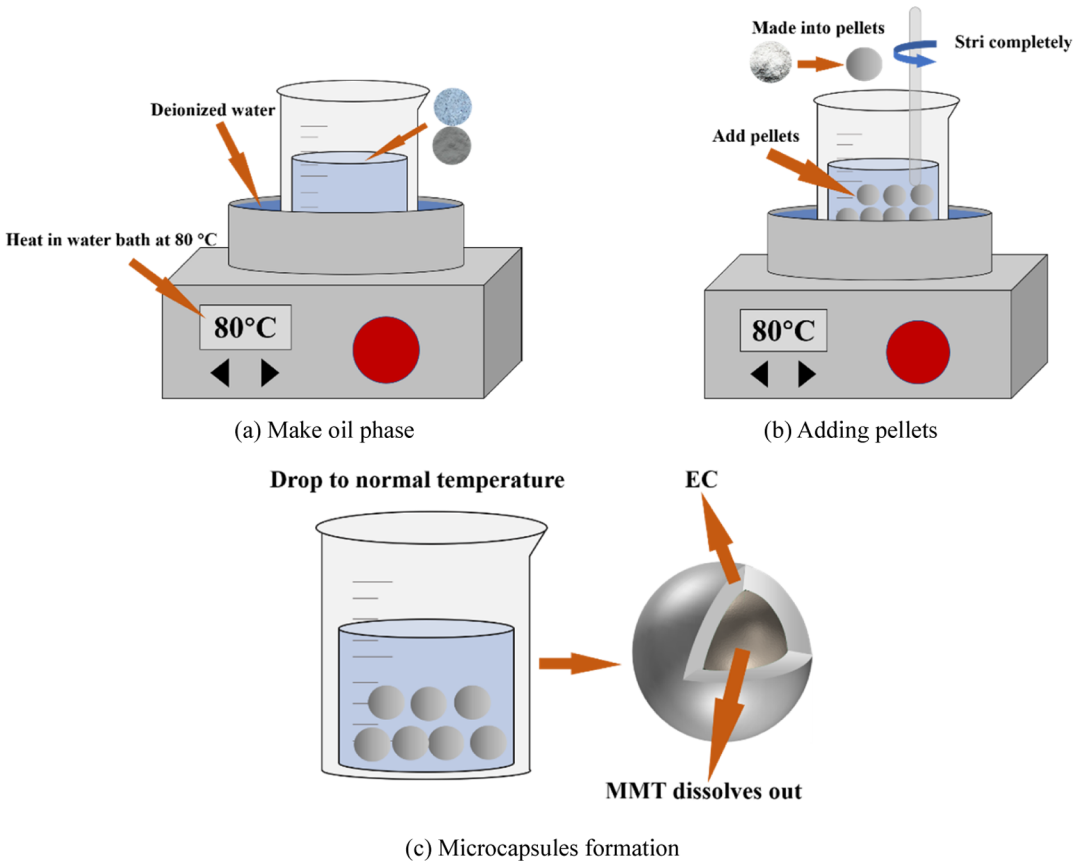

Figure 1. Preparing MMT—EC microcapsules. Modified from ref 45.

developed a new organic polymer sealing material to match this method. Cheng et al.[36] developed a flexible gel (FG) material suitable for borehole deformation to prevent the gas leakage caused by the development and connection of fractures around the gas extraction borehole. Although some new technologies and materials for sealing the fractures around the boreholes have emerged, not only have they increased the difficulty and cost of operation but also the material does not have enough strength and cannot provide enough support and reinforcement around the borehole. The limitations of these materials are especially prominent in soft coal seams with a high gas content. Therefore, researchers focused on the modification of cement-based materials. Liu et al.[37] concluded that the optimal ratio of cement-based materials to water was 1:0.8 and developed a new sealing method to improve gas extraction efficiency. Xiang[38] mixed cement with chemical additives as the raw material for a new cement-based sealing material used in the Fair coal mine. Zou[30] developed a PD sealing material by adding a swelling agent and polymer to the cement. Li et al.[39] developed a new inorganic borehole sealing material with high density and expandability, offering good adhesion to overcome the disadvantages of traditional sealing material, such as poor pore sealing, considerable air leakage, and low extraction concentration. Murtaza et al.[40] studied a novel expandable cement system, and the G-grade cement as a swellable solution to prevent annular flow between the casing and the formation was introduced, with the thought that the swellable solution could be applied in the leakage zone. Wang et al.[41] investigated the air leakage mechanism, discussed the effects of time, active support pressure, and drainage pressure on air leakage, and then proposed a double-expansive (DE) material as the sealant. These sealing materials were cement-based, and then, the expansibility and strength of cement were modified by additives. However, Guanhua et al.[42] proved that the expansion of the aforementioned materials mainly occurred in the early stage as their strength was so low in the initial stage of hydration that the expansion effect induced by the materials could not be maintained: they shrink after solidification, so the expansion effect is significantly reduced. Therefore, selecting the suitable expansion material to allow the expansive component to expand at the appropriate time to seal fractures around the borehole and optimize the strength and expansivity warrants investigation.

Based on cement-based sealing materials, in the present research, microencapsulation technology was applied to wrap the expansive component, thus delaying its expansion. Compared with those of the ordinary expansive materials, the comprehensive properties of expansive delayed materials were investigated from the aspects of expansivity, mechanical properties, and the simulated grouting effect.

2. EXPERIMENTAL PROCEDURE

2.1. Experiment Preparation. *2.1.1. Selection of New Materials.* The expansive cement-based sealing material is currently the most widely used sealing material. Based on the existing borehole sealing material shortcomings, a borehole sealing material should have the following advantages: (1) the sealing material has good compressive strength; (2) the sealing material has good expansivity and the expansion occurs at the appropriate time; (3) the sealing material has a high density, preventing the escape of gas from fractures; and (4) the sealing material is non-toxic, cheap, and workable.

https://doi.org/10.1021/acsomega.2c05628
ACS Omega 2022, 7, 47821−47831

The solubility of ethyl cellulose (EC) in cyclohexane decreases with temperature. It is almost insoluble in cyclohexane at room temperature, resulting in a condensed phase that adheres tothe surface of montmorillonite (MMT). With continuous accumulation, polyethylene (PE) dissolves in cyclohexane, which promotes phase separation and microcapsule formation according to the principle of polymer purification.[43,44] The technology of microcapsule preparation by the oil phase isolation method was introduced, where EC was used as the microcapsule wall material, MMT was used as the microcapsule core material, epoxy resin (ER) was used as the polymer, and PE was used as an additive. The core release process and sustained release effect of the MMT−EC microcapsule were investigated. EC is a type of semisynthetic polymer material, a cellulose derivative, and is a commonly used coated material in water-soluble core materials. It is insoluble in water and has good chemical stability, high mechanical strength, cold resistance, heat resistance, strong alkali resistance, and good film-forming properties. MMT is a fine white or light blue particle, about 0.2 to 1 μm in diameter. It has the characteristics of colloidal dispersion and is usually produced as lumpy or earthy aggregates with a density of about 2 g/cm^3, with strong water absorption, cation exchange capacity, and volumetric expansion of several times to a dozen times after water absorption. PE is a thermoplastic resin generated by the polymerization of ethylene. PE is supplied as odorless, non-toxic, and chemically stable milky particles, which feel like wax to the touch, with a density of about 0.920 g/cm^3.

2.1.2. Preparation Process of Microcapsules. The technique used for preparing the MMT−EC microcapsule is shown in Figure 1. First, EC, PE, and cyclohexane were placed in a three-necked flask, and the reaction device was fixed. Then, we turned on the electric mixer, and the mixed system consisting of EC−PE−cyclohexane was heated in a water bath at 80 °C to dissolve the EC and PE. The MMT was transformed into pellets of the same particle size using ER. The pellets were placed into the mixed system and stirred to blend before another 30 min of stirring was applied at a certain angular velocity to distribute the fine particles of the core material in this mixed system. After that, the mixed system was left to cool in the water bath to ambient temperature. As the solubility of EC decreases, it will gradually condense and precipitate on the surface of the MMT to form MMT−EC microcapsules. After these microcapsules cool to room temperature and solidify, we decrease the suction filtration and use cyclohexane to clean them three times before oven-drying at 40 °C.

2.2. Key Parameters of Microcapsule Preparation. *2.2.1. Determination of EC Dosage.* The solubility of EC in cyclohexane decreases with the temperature, and the condensed phase occurs at room temperature, which adheres to the MMT surface and keeps accumulating. PE dissolves in cyclohexane to promote phase separation and the formation of microcapsules based on the principle of polymer purification. EC is a thermoplastic non-ionic cellulose ether in this research, and the EC with 48−49.5% ethoxy groups was used. The condensed phase generated by the oil phase isolation method should have the properties of a liquid to allow it to flow around the core materials, which requires that the surface tension of the condensed phase should be less than that of the core material, thus allowing complete encapsulation. Experimental investigations showed that with the increase of the EC dosage, the surface tension also increases; however, in the case of excessive EC dosage, EC cannot thoroughly moisten the surface of the capsule core, and the microcapsule itself also tends to adhere. The EC with different dosages was selected, and its encapsulation rate was measured to investigate the effect of EC dosage on the encapsulation rate. The experimental results are shown in Figure 2.

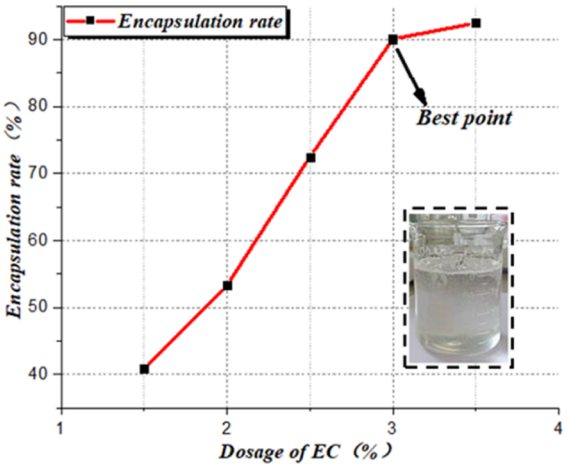

Figure 2. Effect of different EC dosages on the encapsulation rate.

EC dosage plays a vital role in the formation of microcapsules. The effect of different EC dosages on the encapsulation rate of microcapsules is shown in Figure 2. The encapsulation rate increases with the increasing EC dosage because the surface tension of EC will increase with the growth of dosage in cyclohexane solution. The encapsulation rate is a key parameter in the preparation process of microcapsules. The encapsulation rate represents the possibility of leakage of core materials from the inside. EC is more likely to be precipitated out, and its encapsulation rate also increases during phase separation. However, when the added dose of EC was excessive, the encapsulation rate was affected, and thus, the particle size of the microcapsule was also affected. When the dosage of EC exceeded 3%, the growth curve of the encapsulation rate tended to flatten, mainly because the excessive addition makes it difficult for EC to dissolve entirely in cyclohexane. The optimal dosage of EC was determined to have been 3% with the above factors [the percentage (%) sign represents the mass fraction, and the percent sign below is the mass fraction by default].

2.2.2. Determination of the Stirring Speed. When forming the microcapsule, the stirring speed is a key factor affecting the system's uniformity and the core's distribution. Meanwhile, the encapsulation effect, the particle size of microcapsules, and so on will also be affected. Therefore, selecting an appropriate stirring rate in the preparation process is necessary. The changes in the encapsulation rate and particle size of microcapsules at different stirring speeds are shown in Figure 3 by keeping all other variables constant in the preparation process.

Analysis of the effect of different stirring speeds on microcapsules is shown in Figure 3. When the stirring speed is too slow, the core material cannot be floated entirely in the condensed phase, which eventually leads to a larger particle size and an uneven distribution. As the stirring speed increases, the initial condensed phase gradually stabilizes, and the core

https://doi.org/10.1021/acsomega.2c05628
ACS Omega 2022, 7, 47821−47831

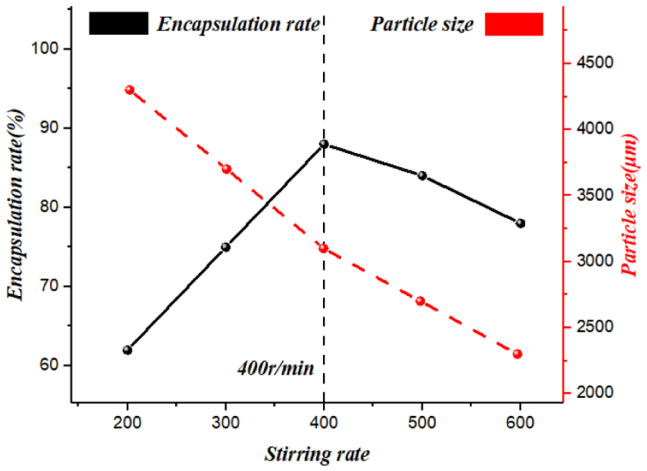

Figure 3. Effect of different stirring speeds on microcapsules.

material can be uniformly dispersed to form microcapsules of uniform particle size. When the stirring speed is excessive, the encapsulation rate will be affected because too fast a stirring rate is not conducive to the adsorption of the wall material on the core material, resulting in many hollow microcapsules. Therefore, 400 rpm was selected as the ideal stirring speed.

2.2.3. Determination of the Optimal Dosage of the Expansion Agent. Different dosages of delayed-expansion materials were used to prepare the cement samples to investigate the optimal additive amount of the delayed-expansion materials. We measured their porosity and rate of expansion. The additive amount of the expansive agent was selected as the independent variable, and cement samples' porosity and expansion rate were chosen as investigation indices. The mix ratio of cement mortar is cement/sand/water = 1:2:0.4. The prepared cement samples were cured at a constant temperature for 28 days after demolding (at a temperature of 22 °C and a relative humidity of 90%). After curing, the cement specimens were dried and weighed (mass M_1), and the mean value (M_0) was calculated. Next, the cement specimens were placed in a vacuum chamber that was then evacuated to vacuum. After that, we immersed them in water until saturated; the cement specimens were then removed from the water; the mass (M_2) was immediately recorded; and the average value M_C was calculated to investigate the effect of different dosages of the expansive delayed agent on the porosity and rate of expansion. The porosity of concrete was calculated using eq 1[46]

$$P = \frac{(M_c - M_0)\rho_c}{M_c\rho_w} \quad (1)$$

where M_c is the average value of the wet mass after water absorption in kilograms; M_0 is the average value of the dry mass in kilograms; ρ_w is the density of water at room temperature in kilograms per cubic meter; and ρ_c is the apparent density after water absorption in kilograms per cubic meter.

Expansivity plays a vital role in the sealing property of sealing materials. An appropriate expansion volume and expansion time of the sealing material is one of the essential ways to compensate for the shrinkage of the cement-based material in later periods and its uneven density. In this experiment, MMT was used as the expansive agent of the cement material. It is a monoclinic laminated clay material. The main structure contains a silicon-oxygen tetrahedron and aluminum−oxygen octahedra. In the structure of MMT, both sides of the crystal layer are composed of oxygen molecules. The force between the crystal layers is an intermolecular force (there is no hydrogen bonding therein), which is conducive to water infiltration. On the other hand, because MMT contains multiple lattices, these provide many exchangeable cations on the crystal surface. After water molecules enter the crystal layer, these exchangeable cations dissociate in water and form a diffused double electric layer, which gives the crystal surface a negative charge, and mutual repulsion ensues, thus endowing the MMT with water absorption and expansivity.

As shown in Figure 4, the porosity and expansion ratio of the material increase with the dose of the additive agent: however,

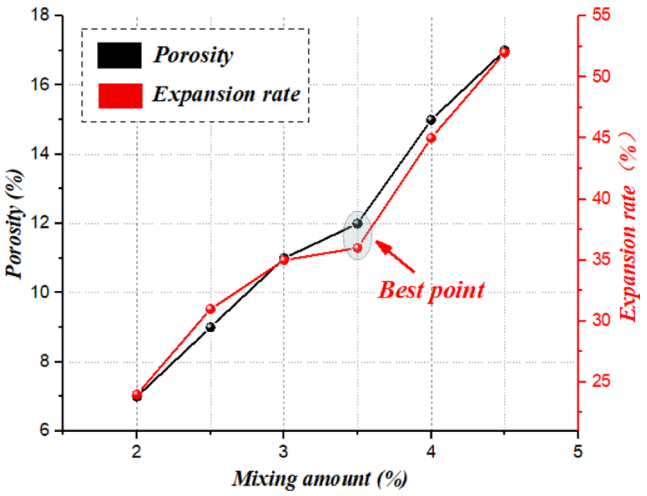

Figure 4. Effect of the mixing amount on microcapsules.

excessive expansion of the material will result in the formation of many holes and primary cracks inside the material, resulting in poor sealing performance. Therefore, a reasonable dosage of the expansion agent is very important. When the dosage of the expansive agent is between 3 and 3.5%, the porosity and expansion rate decrease: macropores generated in the initial stage are gradually transformed into micropores due to the continuous expansion of the material. Herein, this is defined as the stage of pore transformation, in which the expansion rate and porosity can ensure the optimal sealing performance of the material. The ideal dose of the expansion agent is 3.5%.

2.2.4. Effect of the CWR on the Sustained Release of Microcapsules. The CWR is the ratio of the core material wrapped inside the microcapsule to the outer wall material. The release time of the core material mainly depends on the CWR. The smaller the CWR, the slower the dissolution of the microcapsules. The main component of the core material is MMT, and the wall material is EC. The CWRs were selected as variables, and the rate of dissolution of microcapsules under different CWRs was investigated.

The relationship between the CWR and the sustained release of microcapsules is shown in Figure 5. The dissolution rate curve can be divided into the delay, release, and final stages. The microcapsule core material release is insignificant, with almost nothing released, as the wall material dissolves in the delay stage. The smaller the CWR, the thicker the wall of microcapsules, and the longer the action time of delayed release. In the release stage, the wall material dissolves and

https://doi.org/10.1021/acsomega.2c05628
ACS Omega 2022, 7, 47821−47831

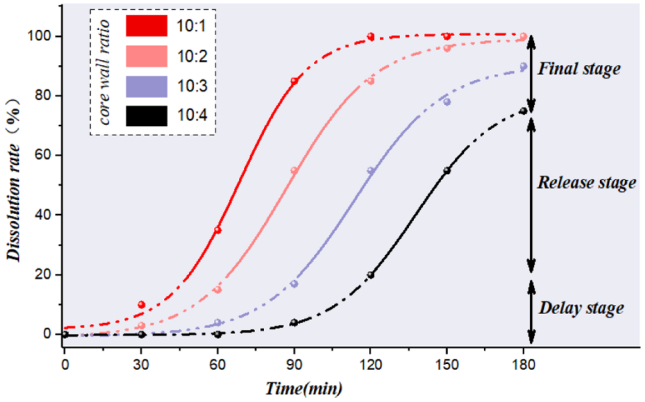

Figure 5. Effect of the CWR on sustained release.

releases a large amount of the core material. Under the function of the expansive agent, the cement-based material begins to expand significantly. In the final stage, the core material is nearly all released, and the cement-based material stops increasing and has enough strength. The dissolution rate is an important parameter of the delayed sealing material in the actual hole sealing work. Considering that workers will spend a certain amount of time in batching, pipe laying, and grouting during the downhole drilling and sealing work and that it also takes time for cement solidification to have a certain strength, delaying the release period of the expansion sealing material will effectively avoid a large waste of the expansion energy of the expansion component in the early stage of hydration.

When the ratio of the core to the wall is 10:1, the delayed release of microcapsules is the worst, and the release of the core material is almost completed within 90 min. The strength of the cement-based material is then too low, and the premature release of the core material does not affect the volumetric expansion of the material. When the CWR is 10:4, the time for the core material to be released is too long, and the release effect is poor, thus failing to achieve the expected impact of the experiment. When the CWR is 10:3, expansive components are released within 90 to 135 min: the cement has sufficient strength, thereby achieving coordinated development of expansion and strength behaviors. In conclusion, the CWR of 10:3 is deemed optimal.

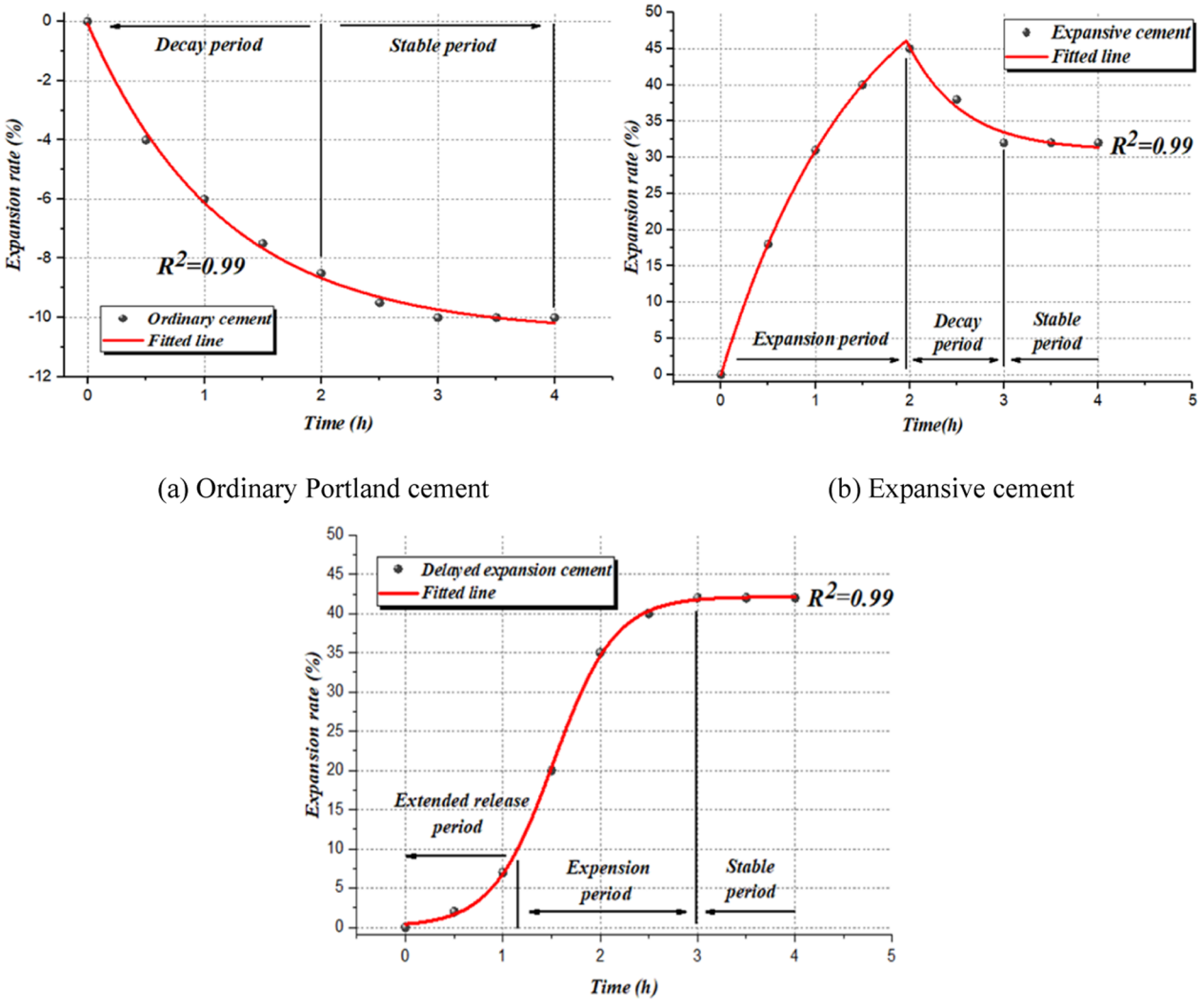

Figure 6. Volume change curves of the ordinary Portland cement, expansive cement, and delayed-expansion cement.

https://doi.org/10.1021/acsomega.2c05628
ACS Omega 2022, 7, 47821−47831

Table 1. Test Results and Parameters of Samples under Different Confining Pressures

specimen	specimen no.	confining pressure/MPa	peak intensity/MPa	peak strain/%	elastic modulus E/GPa
delayed-expansion cement	DE-1	1	20.92	0.65	5.263
	DE-2	3	26.28	0.93	6.032
	DE-3	5	30.34	1.25	6.728
expansive cement	OE-1	1	17.12	1.03	2.708
	OE-2	3	21.78	1.24	2.936
	OE-3	5	26.52	1.45	3.872

3. PERFORMANCE TESTING OF DELAYED-EXPANSION SEALING MATERIALS

3.1. Expansion Performance Test. Considering the high requirements of the drilling sealing materials for the expansion performance, the expansion of the material is as follows

$$\alpha = (M_1 - M_0)/M_0 \quad (2)$$

where α is the rate of the volume change of the material (%); M_0 is the initial volume of the material (m^3); and M_1 is the final volume of the material (m^3).

Since expansivity is an important indicator used to evaluate the performance of borehole sealing materials, delayed-expansion microcapsule cement was used in the experimental group, and expansive cement and ordinary cement were used in the control group. The water−cement ratio of the three groups was set to 0.6:1. Mixes were stirred evenly and then poured into transparent beakers to facilitate the measurement of the changes in the volume of the materials. The volume change with different materials is shown in Figure 6. The fitting equations are as follows

$$\text{expansion rate} = 10.49 \times e^{-h/1.15} - 10.55 \quad (a)$$

$$\text{expansion rate} = \begin{cases} 46.29 + 65.34(e^{-1.24} - e^{-h/1.57}), & h \le 1.94 \\ 31.88 + 14.41e^{-h-1.94/1.63}, & h > 1.94 \end{cases} \quad (b)$$

$$\text{expansion rate} = \frac{42.22}{1 + e^{-3.05(h-1.52)}} \quad (c)$$

3.2. Mechanical Property Measurement. This study used the electro-hydraulic triaxial servo test system (MTS815) to conduct triaxial compression tests on cement specimens. This system mainly comprises a loading system, a measuring system, and a control system. The maximum axial load, confining pressure, and sensitivity of the servo valve are 4600 kN, 140 MPa, and 290 Hz, respectively, and the minimum sampling time is 50 μs. All operations were axial displacement-controlled at a rate of 0.001 mm/s until the specimens underwent complete failure. High-precision sensors were chosen for data acquisition to ensure the reliability of experimental data.

Before the experiment, delayed-expansion sealing material and ordinary expansion sealing material were poured into standard molds measuring 70 mm × 70 mm × 70 mm to produce specimens A and B. These were then demolded and placed in the curing tank for 28 days. The electro-hydraulic triaxial servo test system (MTS815) was applied to measure the mechanical properties of two cement samples under different confining pressures (1, 3, and 5 MPa). Each sample was repeated under the same conditions, and the average value was taken. The results are shown in Table 1. The experimental equipment is shown in Figure 7. The stress−strain curves of

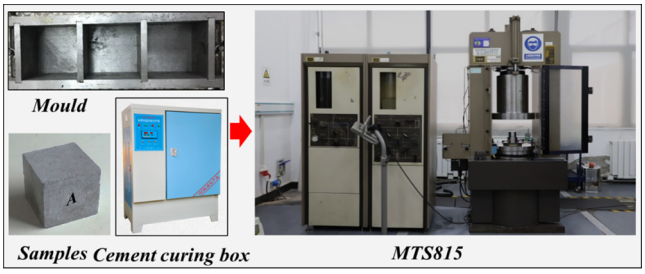

Figure 7. Electro-hydraulic triaxial servo test system.

two types of specimens under different confining pressures are shown in Figure 8, through which the peak strength and strain of the material can be obtained. In addition, the material's elastic modulus (E) can be obtained from the analysis of the stress−strain curves at the elastic deformation stage.

3.3. Laboratory Simulation of Grouting. A test bed for simulating borehole sealing was established to verify the sealing performance of delayed-expansion sealing material. The delayed-expansion sealing material and ordinary expansion cement were used to seal the borehole to investigate microstructural differences in coal samples around the borehole after grouting.

(1) Steel molds measuring 400 mm × 400 mm × 400 mm were prepared to fix the coal samples. The coal samples were divided into two groups (A and B). Then, we filled the molds with coal samples. After that, we drilled a simulated borehole with a diameter of 40 mm and a length of 40 mm in the center of the sample surface (Figure 9). Next, the delayed-expansion sealing material and ordinary expansion material were used to seal the simulated borehole. The laboratory temperature was 25 °C, and the relative humidity was 95%. After the two sealing materials expanded and solidified, the borehole sealing model of a gas extraction borehole was completed.

(2) To facilitate the observation of the sample, we cut apart the borehole sealing model in the radial direction along the borehole. We selected samples with a diameter of 10 mm (after solidification), putting them into a vacuum device for vacuum treatment, and then immersed them in distilled water for 48 h until saturated. Low-field nuclear magnetic resonance (NMR) was applied to measure the T_2 relaxation time of the samples. The main magnetic field strength of the equipment was 0.51 T, the temperature (T) of the magnet was set to 35 °C, the number of scans (NS) was set to 128, and the echo time (T_E) was 0.2 ms. The T_2 spectrum of each sample was obtained through analysis, which can be used to assess

https://doi.org/10.1021/acsomega.2c05628
ACS Omega 2022, 7, 47821−47831

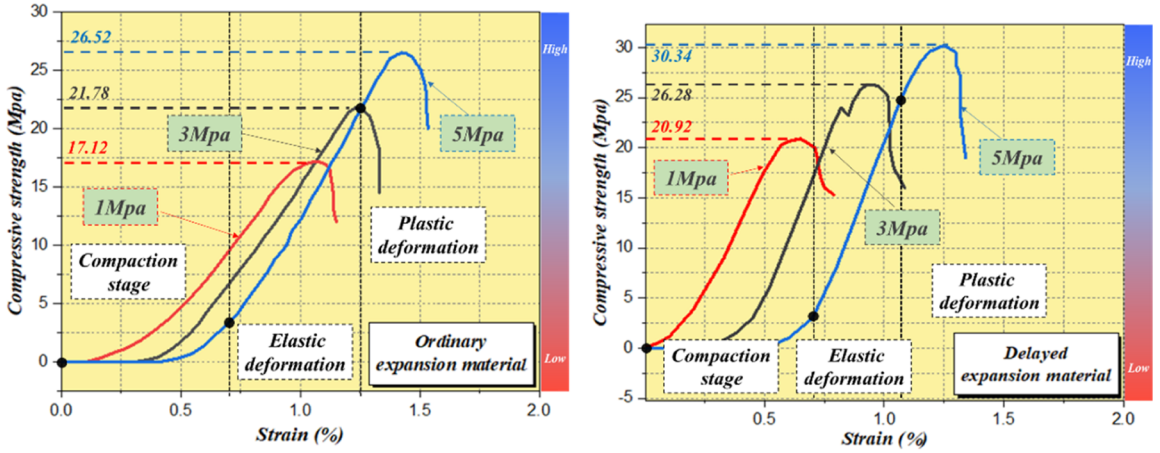

(a) expansive cement (b) delayed-expansion sealing material

Figure 8. Stress−strain curves of specimens.

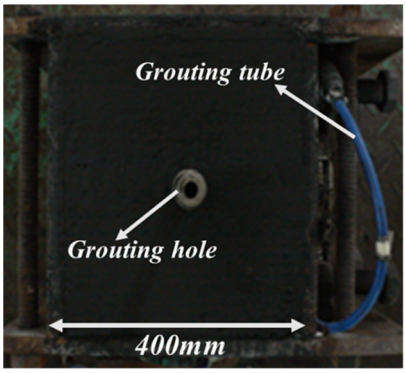

Figure 9. Experimental simulated borehole.

the changes in the amounts of various pores in the coal sample.

The value of transverse relaxation time (T_2) reflects the pore size of the sample, and the relationship between the pore size (r) of coal and the transverse relaxation time (T_2) in NMR can be expressed as[47]

$$r = T_2 F_s \rho \tag{3}$$

where r is the pore radius (μm). T_2 is the NMR transverse relaxation time (ms). ρ is the surface relaxation rate (μm/mm). F_s is the pore shape factor, and the significance of introducing this parameter is to distinguish different shapes or types of pores.

The smaller the value of T_2, the smaller the pore size of the corresponding pore. In this experiment, Carr−Purcell−Meiboom−Gill sequence signal data of samples were obtained by low-field NMR scanning. Then, the T_2 spectrum distribution was obtained by inversion, allowing analysis of the pore characteristics. In the experiment, two sealing materials were used to simulate the grouting of a borehole. After that, the coal samples obtained at 50 and 100 mm from the borehole were taken for analysis: T_2 spectra of coal samples taken at different distances from the borehole wall are shown in Figure 10.

4. RESULTS AND DISCUSSION

4.1. Analysis of Expansion Properties. Based on the volume change curves of the three kinds of borehole sealing materials, taking derivatives of the volume change curves, the change in the rate of expansion of different materials at different periods was obtained (Figure 11). Figures 6 and 11 show that the expansion properties of the different sealing materials at different periods are quite different.

It can be found from Figures 6a and 11 that the setting time of cement is 4 h and the final rate of volumetric change of ordinary cement material is −10%. Because the cement slurry contains much moisture in the initial stage: during solidification, the volatilization of water will cause shrinkage of the material, which generates multiple cracks inside the material and reduces its sealing performance. Since cement itself cannot expand, it can only rely on the grouting pressure and fluidity to seal the borehole during grouting. However, the material in the borehole will shrink after solidification, thereby generating multiple cracks in the upper part of the borehole, reducing the sealing effect.

Based on ordinary cement, the final volume is increased by 32% compared with the initial in the addition of an expansion agent to prevent shrinkage of the material. The expansion process of ordinary expansive cement material can be divided into three periods, as shown in Figure 6b: an expansion period, a decaying-expansion period, and a stable period. The material begins to expand rapidly in the initial stage of the hydration reaction so that the expansion volume of the slurry reaches its maximum after 2 h. Then, the volume begins to decrease until the slurry solidifies. When the reaction is nearly ended, the cement slurry cannot store the internal expansion energy due to its insufficient strength and ultimately cannot achieve the best sealing effect. Figure 11 shows that the volume growth rate of ordinary cement is the fastest in the initial reaction stage and then decreases. The volume change rate becomes negative after 2 h of the reaction because the expansive components inside the material have been consumed, but the material has not solidified. Therefore, the material reaches the volume decay period again. A large amount of the previous expansion would be re-released, resulting in ineffective expansion. In addition, a large amount of gas generated in the initial stage of the reaction will lead to rapid expansion. After releasing this expansion energy, the material will begin to contract due to a lack of strength, leading to increased porosity and micro-cracking in the material, thus reducing its density. Moreover, the large amount of gas formed in the initial stage of

https://doi.org/10.1021/acsomega.2c05628
ACS Omega 2022, 7, 47821−47831

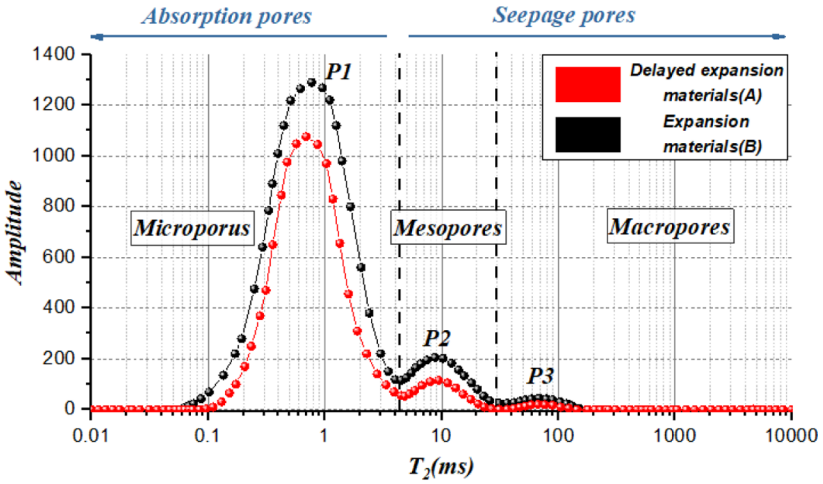

(a) T_2 spectra of coal samples taken 50 mm from the borehole wall

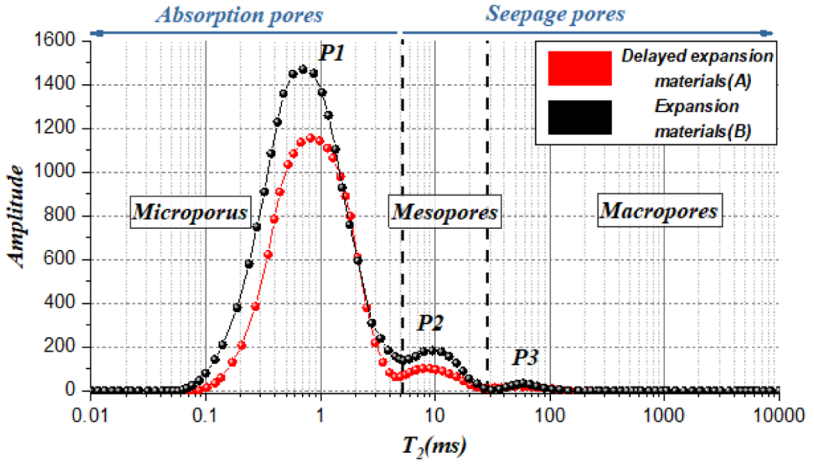

(b) T_2 spectra of coal samples taken 100 mm from the borehole wall

Figure 10. T_2 spectra of coal samples taken at different distances from the borehole wall.

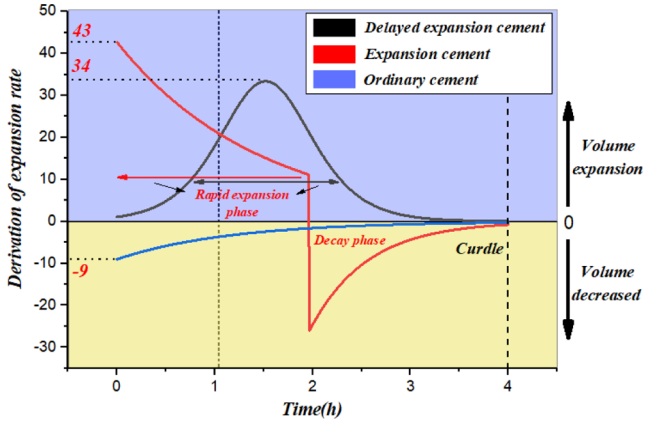

Figure 11. Rate of volume change.

the reaction will result in the rapid expansion of the material. When the expansion energy is dissipated, the material will shrink due to its insufficient strength.

Using expansive cement, MMT is used to replace aluminum powder as an expansion agent to envelop the expansion agent and delay its effect by microcapsule technology. As seen in Figure 6c, the delayed-expansion cement volume evolution curve can be divided into three periods: delayed release, expansion, and stable. Under the delayed release effect, the material's volume change an hour before the reaction is not apparent, but the delayed release effect is significant. Within 2.5 h after the reaction, the expansion rate becomes stable, and the final volume expansion rate increases to 42%. As seen from Figure 11, the values at both ends of the curve are low, while the values in the middle are high, reflecting the characteristics of a normal distribution. The volume expansion of the material mainly occurs within 0.8 to 2.2 h after the reaction, and the expansive internal components of the microcapsules enter the cement hydration environment. The hydration products react with the expansion agent to form a large amount of gas, resulting in a delayed expansion to achieve coordinated development of expansion and strength. The delayed-expansion material grouting can better seal the cracks around the borehole instead of only relying on the grouting pressure.

4.2. Analysis of Stress−Strain Curves. The stress−strain curves of specimens A and B under different confining pressures are shown in Figure 8. The curve can be divided into three stages: (1) compaction stage. This stage is the initial loading stage, where cracks caused by the cement shrinkage gradually close under the load and the density of the material increases. (2) Elastic deformation stage. In this stage, cracks

https://doi.org/10.1021/acsomega.2c05628
ACS Omega 2022, 7, 47821−47831

begin to develop slowly inside the material, and a small number of cracks appear near the critical point. (3) Plastic deformation stage. In this stage, multiple longitudinal cracks appear on the sample's surface, and horizontal cracks also evolve rapidly; the sample's integrity begins to be degraded.

The following can be concluded from Figure 8a,b:

(1) Compared with ordinary expansive cement, delayed-expansion sealing materials have better mechanical properties. When the confining pressure is 1, 3, and 5 MPa, the corresponding peak strength is increased by 22.2, 20.7, and 14.5%, respectively, indicating that the delayed-expansion sealing material provides better compressive performance.

(2) The peak strength and maximum axial strain of the two materials increase with the confining pressure. The greater the confining pressure, the greater the peak strength and the maximum axial strain. The increased confining pressure will allow the material to reach the plastic deformation stage more slowly. When the confining pressure increases from 1 to 3 MPa, the peak strength of the two materials increases by 25.62 and 27.22%, respectively. When the confining pressure increases from 3 to 5 MPa, the peak strength of the two materials increases by 15.45 and 21.76%, respectively. This is because the internal cracks and pores are more compacted during this stage. Moreover, the peak strength increment of the delayed-expansion sealing material under different confining pressures is smaller than that of ordinary expansion sealing material.

(3) Compared with ordinary expansion materials, delayed-expansion sealing materials have a shorter compaction stage. When the confining pressures are 1, 3, and 5 MPa, the peak strains of delayed-expansion sealing material decrease by 39.25, 25, and 13.79%, respectively, indicating that the porosity and fracture content of the specimen decrease and the material is denser. The elastic deformation stage of the delayed-expansion sealing material is longer, which proves that there is more stored elastic strain energy in the material, and the material is more resistant to external damage.

Triaxial compression experiments showed that delayed-expansion cement has improved physical properties compared with ordinary cement. Under different confining pressures, delayed-expansion cement samples exhibit higher peak stress (increasing by 19.13% on average). This is because, in the solidification stage, the delayed-expansion cement achieves a coordinated development of expansion and strength, thus avoiding the problem of an uneven distribution of pores within the material, thus densifying the material.

4.3. Analysis of NMR Spectra. It can be seen from the T_2 spectra of the coal samples at different distances from the borehole wall that the coal samples grouted using other sealing materials have significant differences. According to formula (3), the transverse relaxation time (T_2) is proportional to the pore size in a coal sample (R); the longer the T_2 is, the larger the pore size is. The T_2 spectrum can reflect the distribution of pore sizes in coal samples. The closer the coal sample is to the borehole wall, the higher the peak value is in the T_2 spectrum and the more the cracks develop inside the material. It can be seen from Figure 10 that for coal samples A and B that use different sealing materials for grouting at the same location, the three peak values of specimen A are all lower than those of specimen B, and the widths of the initial T_2 of each peak for specimen A (grouted by the delayed-expansion sealing material) all decrease. The amounts of macropores and mesopores inside the two sealing materials (Figure 12) are

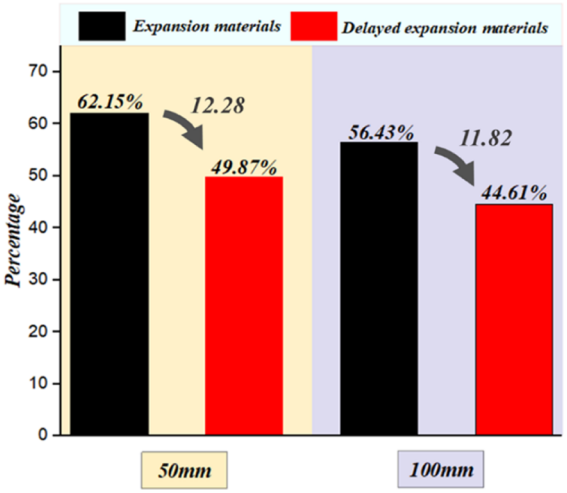

Figure 12. Macropore and mesopore contents of the two sealing materials.

calculated from data in Figure 10. It can be seen from Figure 12 that the proportion of mesopores and macropores some 50 mm from the borehole wall decreases from 62.15 to 49.87% and that of mesopores and macropores inside the coal sample taken 100 mm from the borehole wall decreases from 56.43 to 44.61%, indicating that the delayed-expansion sealing material provides a better sealing effect than the ordinary expansion material. The main reason for this is that the ordinary expansion material begins to expand during the initial stage of the grouting process. Then, it gradually shrinks, so the material cannot fill the fractures around the borehole. Moreover, the volumetric shrinkage will result in the formation of pores and cracks in the material, thereby reducing its density. However, the delayed-expansion sealing materials can expand at the appropriate time to ensure that the material can actively expand before reaching a certain strength to achieve coordinated development of expansion and strength. Finally, the cracks around the borehole can thus be effectively sealed.

5. CONCLUSIONS

We used MMT as an expansive agent based on traditional cement-based sealing materials. In addition, we applied microencapsulation technology to wrap the expansive component of the sealing material to develop delayed-expansion microcapsules. The key parameters of the delayed-expansion capsule and its delayed release process were investigated through experiments, and the mechanical and microscopic properties were studied. The main conclusions are as follows:

(1) The expansion member will expand at an appropriate time under the action of delayed expansion microcapsules, and the most satisfactory results are achieved when the EC content is 3%, the stirring speed is 400 rpm, and the MMT content is 3.5%

(2) The delayed expansion material swells significantly within 0.8−2.2 h of the hydration reaction. Through microcapsule technology, the delayed release effect

https://doi.org/10.1021/acsomega.2c05628
ACS Omega 2022, 7, 47821−47831

overcomes the problem of premature release and failure of the expansion agent, thereby improving the overall hole sealing performance.

(3) The delayed-expansion sealing material has better mechanical properties. Its peak stress was increased by 19.13% (on average) under different confining pressures, which proves that the material can improve the stability of the borehole. In addition, the peak strains under other confining pressures were reduced by 39.25, 25, and 13.79%, respectively, compared with ordinary expansive cement, which indicated that the delayed expansion material increased in density and decreased in internal pores and fissures.

(4) The NMR scan of the coal sample injected with ordinary expansion materials and delayed-expansion sealing materials shows that the proportions of macropores and mesopores in the total pore volume in the coal sample taken some 50 mm from the borehole wall decreased from 62.15 to 49.87% and those in specimens sampled at 100 mm from the borehole wall decreased from 56.43 to 44.61%. It is indicated that the delayed-expansion sealing material is more tightly sealed.

AUTHOR INFORMATION

Corresponding Author

Zhang Chao − *College of Safety Science and Engineering, Xi'an University of Science and Technology, Xi'an, Shanxi 710054, China*; Email: zc@xust.edu.cn

Authors

Qin RongRong − *College of Safety Science and Engineering, Anhui University of Science and Technology, Huainan, Anhui 232001, China; School of Safety Engineering, China University of Mining and Technology, Xuzhou, Jiangsu 221116, China*

Jiang Bingyou − *College of Safety Science and Engineering, Anhui University of Science and Technology, Huainan, Anhui 232001, China*

Liu Ting − *School of Safety Engineering, China University of Mining and Technology, Xuzhou, Jiangsu 221116, China*; orcid.org/0000-0002-1636-5990

Chang Jie − *College of Safety Science and Engineering, Xi'an University of Science and Technology, Xi'an, Shanxi 710054, China*

Fan Fuhuai − *College of Safety Science and Engineering, Xi'an University of Science and Technology, Xi'an, Shanxi 710054, China*

Complete contact information is available at: https://pubs.acs.org/10.1021/acsomega.2c05628

Notes

The authors declare no competing financial interest.

ACKNOWLEDGMENTS

This work was financially supported by the National Natural Science Foundation of China (grant nos. 52174203, 51974241, and 51874233).

REFERENCES

(1) Wang, G.; Wu, M.; Wang, R.; Xu, H.; Song, X. Height of the mining-induced fractured zone above a coal face. *Eng. Geol.* **2017**, *216*, 140−152.

(2) Wang, H.; Nie, W.; Cheng, W.; Liu, Q.; Jin, H. Effects of air volume ratio parameters on air curtain dust suppression in a rock tunnel's fully-mechanized working face. *Adv. Powder Technol.* **2018**, *29*, 230−244.

(3) Wang, B.; Hu, Z. Statistical analysis and regularity analysis of coal mine gas explosion accidents. *Coal Technol.* **2022**, *41*, 148−151.

(4) Xue, S.; Wang, Y.; Xie, J.; Wang, G. A coupled approach to simulate initiation of outbursts of coal and gas—Model development. *Int. J. Coal Geol.* **2011**, *86*, 222−230.

(5) Wang, L.; Cheng, Y.; Wang, L.; Guo, P.; Li, W. Safety line method for the prediction of deep coal-seam gas pressure and its application in coal mines. *Saf. Sci.* **2012**, *50*, 523−529.

(6) Zhao, L.; Guanhua, N.; Lulu, S.; Qian, S.; Shang, L.; Kai, D.; Jingna, X.; Gang, W. Effect of ionic liquid treatment on pore structure and fractal characteristics of low rank coal. *Fuel* **2020**, *262*, 116513.

(7) Liu, Q.; Nie, W.; Hua, Y.; Peng, H.; Liu, C.; Wei, C. Research on tunnel ventilation systems: Dust Diffusion and Pollution Behaviour by air curtains based on CFD technology and field measurement. *Build. Environ.* **2019**, *147*, 444−460.

(8) Tang, J.; Wang, C.; Chen, Y.; Li, X.; Yang, D.; Liu, J. Determination of critical value of an outburst risk prediction index of working face in a coal roadway based on initial gas emission from a borehole and its application: A case study. *Fuel* **2020**, *267*, 117229.

(9) Liu, H.; Liu, H.; Cheng, Y. The elimination of coal and gas outburst disasters by ultrathin protective seam drilling combined with stress-relief gas drainage in Xinggong coalfield. *J. Nat. Gas Sci. Eng.* **2014**, *21*, 837−844.

(10) Xiaocun, C.; Hui, T. Technical scheme and application of pressure-relief gas extraction in multi-coal seam mining region. *Int. J. Min. Sci. Technol.* **2018**, *28*, 483−489.

(11) Yao, B.; Ma, Q.; Wei, J.; Ma, D.; Cai, D. Effect of protective coal seam mining and gas extraction on gas transport in a coal seam. *Int. J. Min. Sci. Technol.* **2016**, *26*, 637−643.

(12) Yang, F.; Li, P.; Su, W.; Zhang, J.; Wang, L.; Guo, T.; Wang, X. Study on reasonable gas extraction radius based on multi-index and multi-method. *Energy Rep.* **2022**, *8*, 287−294.

(13) Junxiang, Z.; Bo, L.; Yuning, S. Dynamic leakage mechanism of gas drainage borehole and engineering application. *Int. J. Min. Sci. Technol.* **2018**, *28*, 505−512.

(14) Erol, S.; François, B. Efficiency of various grouting materials for borehole heat exchangers. *Appl. Therm. Eng.* **2014**, *70*, 788−799.

(15) Li, D. A new technology for the drilling of long boreholes for gas drainage in a soft coal seam. *J. Petrol. Sci. Eng.* **2016**, *137*, 107−112.

(16) Junxiang, Z.; Bo, L.; Yuning, S. Dynamic leakage mechanism of gas drainage borehole and engineering application. *Int. J. Min. Sci. Technol.* **2018**, *28*, 505−512.

(17) Zhai, C.; Hao, Z.; Lin, B. Research on a New Composite Sealing Material of Gas Drainage Borehole and Its Sealing Performance. *Procedia Eng.* **2011**, *26*, 1406−1416.

(18) Zhang, Y.; Hu, S.; Xia, T.; Liu, Y.; Pan, Z.; Zhou, F. A novel failure control technology of cross-measure borehole for gas drainage: A case study. *Process Saf. Environ. Prot.* **2020**, *135*, 144−156.

(19) Zhang, X.; Gao, J.; Jia, G.; Zhang, J. Study on the influence mechanism of air leakage on gas extraction in extraction boreholes. *Energy Explor. Exploit.* **2022**, *40*, 1344−1359.

(20) Wang, H.; Yao, Y.; Liu, D.; Pan, Z.; Yang, Y.; Cai, Y. Fault-sealing capability and its impact on coalbed methane distribution in the Zhengzhuang field, southern Qinshui Basin, North China. *J. Nat. Gas Sci. Eng.* **2016**, *28*, 613−625.

(21) Giannoukos, K.; Hall, M.; Rochelle, C.; Milodowski, A.; Rigby, S. Preliminary Investigation on the Chemical Response of Cementitious Grouts Used for Borehole Sealing of Geologically Stored CO_2. *Energy Proc.* **2014**, *59*, 174−181.

(22) Kim, C.; Dixon, D. Evaluating hydro-mechanical interactions of adjacent clay-based sealing materials. *Phys. Chem. Deep Earth* **2013**, *65*, 98−110.

(23) Wang, H.; Wang, E.; Li, Z.; Wang, X.; Zhang, Q.; Li, B.; Ali, M. Study on sealing effect of pre-drainage gas borehole in coal seam

based on air-gas mixed flow coupling model. *Process Saf. Environ. Prot.* **2020**, *136*, 15−27.
(24) Yang, Z.; Zhang, X.; Liu, X.; Guan, X.; Zhang, C.; Niu, Y. Flexible and stretchable polyurethane/waterglass grouting material. *Construct. Build. Mater.* **2017**, *138*, 240−246.
(25) Wang, Z.; Sun, Y.; Li, Z.; Wang, Y.; You, Z. Multiphysics responses of coal seam gas extraction with borehole sealed by active support sealing method and its applications. *J. Nat. Gas Sci. Eng.* **2022**, *100*, 104466.
(26) Guanhua, N.; Qian, S.; Meng, X.; Hui, W.; Yuhang, X.; Weimin, C.; Gang, W. Effect of NaCl-SDS compound solution on the wettability and functional groups of coal. *Fuel* **2019**, *257*, 116077.
(27) Wu, H.; Li, X.; Gao, X.; Chen, D.; Li, Z. Development and Application of Water Sealing Technology for Gas Drainage Boreholes. *ACS Omega* **2022**, *7*, 733−743.
(28) Wang, Z. F.; Zhou, Y.; Sun, Y. N.; Wang, Y. L. Novel gas extraction borehole grouting sealing method and sealing mechanism. *J. China Coal Soc.* **2015**, *40*, 588−595.
(29) Zhang, J.; Zhai, C.; Zhong, C.; Xu, J.; Sun, Y. Investigation of sealing mechanism and field application of upward borehole self-sealing technology using drill cuttings for safe mining. *Saf. Sci.* **2019**, *115*, 141−153.
(30) Zou, Q.; Lin, B.; Zheng, C.; Hao, Z.; Zhai, C.; Liu, T.; Liang, J.; Yan, F.; Yang, W.; Zhu, C. Novel integrated techniques of drilling-slotting-separation-sealing for enhanced coal bed methane recovery in underground coal mines. *J. Nat. Gas Sci. Eng.* **2015**, *26*, 960−973.
(31) Guanhua, N.; Kai, D.; Shang, L.; Qian, S. Gas desorption characteristics effected by the pulsating hydraulic fracturing in coal. *Fuel* **2019**, *236*, 190−200.
(32) Chen, Y.; Li, A.; Yang, D.; Liu, T.; Li, X.; Tang, J.; Jiang, C. Study on the Interaction between Low-Viscosity High-Permeability Pregrouting Sealing Material and Coal and Its Application. *Adv. Polym. Technol.* **2020**, *2020*, 1217285.
(33) Hu, S.; Zhou, F.; Geng, F.; Liu, Y.; Zhang, Y.; Wang, Q. Investigation on blockage boundary condition of dense-phase pneumatic conveying in bending slits. *Powder Technol.* **2014**, *266*, 96−105.
(34) Hao, C.; Cheng, Y.; Dong, J.; Liu, H.; Jiang, Z.; Tu, Q. Effect of silica sol on the sealing mechanism of a coalbed methane reservoir: New insights into enhancing the methane concentration and utilization rate. *J. Nat. Gas Sci. Eng.* **2018**, *56*, 51−61.
(35) Wang, K.; Lou, Z.; Wei, G.; Qin, B.; Wang, L. A novel anti-air-leakage method and an organic polymer material for improving methane drainage performance. *Process Saf. Environ. Prot.* **2019**, *129*, 152−162.
(36) Cheng, Z.; Xu, Y.; Guanhua, N.; Min, L.; Zhiyong, H. Microscopic properties and sealing performance of new gas drainage drilling sealing material. *Int. J. Min. Sci. Technol.* **2013**, *23*, 475−480.
(37) Liu, Q.; Cheng, Y.; Yuan, L.; Fang, Y.; Shi, D.; Kong, S. A new effective method and new materials for high sealing performance of cross-measure CMM drainage boreholes. *J. Nat. Gas Sci. Eng.* **2014**, *21*, 805−813.
(38) Xiang, X.; Zhai, C.; Xu, Y.; Yu, X.; Xu, J. A flexible gel sealing material and a novel active sealing method for coal-bed methane drainage boreholes. *J. Nat. Gas Sci. Eng.* **2015**, *26*, 1187−1199.
(39) Li, Q.; Lin, B.; Zhai, C. A new technique for preventing and controlling coal and gas outburst hazard with pulse hydraulic fracturing: a case study in Yuwu coal mine, China. *Nat. Hazards* **2015**, *75*, 2931−2946.
(40) Murtaza, M.; Tariq, Z.; Rahman, M.; Kamal, M.; Mahmoud, M. Novel Expandable Cement System for Prevention of Sustained Casing Pressure and Minimization of Lost Circulation. *ACS Omega* **2021**, *6*, 4950−4957.
(41) Wang, Z.; Sun, Y.; Wang, Y.; Zhang, J.; Sun, Z. A coupled model of air leakage in gas drainage and an active support sealing method for improving drainage performance. *Fuel* **2019**, *237*, 1217−1227.
(42) Guanhua, N.; Kai, D.; Shang, L.; Qian, S.; Dongmei, H.; Ning, W.; Yanying, C. Development and performance testing of the new sealing material for gas drainage drilling in coal mine. *Powder Technol.* **2020**, *363*, 152−160.
(43) Liu, J.; Chen, Z.; Yao, L.; Wang, S.; Huang, L.; Dong, C.; Niu, L. The 2D platelet confinement effect on the membrane hole structure probed by electrochemical impedance spectroscopy. *Electrochem. Commun.* **2019**, *106*, 106517.
(44) Chen, Y.*Remediation of chlorinated pollution in groundwater by use of controlled-released potassium permanganate*; Fuzhou Universitye, 2010.
(45) Zhang, C.; Fan, F.; Li, S.; Zhai, C.; Jiang, B.; Yang, P.; Zeng, X. Research on gas drainage borehole sealing material based on microcapsule technology. *Int. J. Coal Sci. Technol.* **2021**, *978*, 1−8.
(46) al-Swaidani, A. M. Use of micro and nano volcanic scoria in the concrete binder: Study of compressive strength, porosity and sulfate resistance. *Case Stud. Constr. Mater.* **2019**, *11*, No. e294.
(47) Li, C.; Shen, B.; Lu, L.; Jiang, Q.; Pan, A.; Tao, J.; Ding, J. Pore structure characterization of Shahezi Formation shale in Songliao Basin: Based on low-field nuclear magnetic resonance technology. *Petrol. Reservoir Eval. Dev.* **2022**, *12*, 468−476.

https://doi.org/10.1021/acsomega.2c05628
ACS Omega 2022, 7, 47821−47831